Supplement of Earth Syst. Sci. Data, 13, 5969–5986, 2021
https://doi.org/10.5194/essd-13-5969-2021-supplement

Supplement of

NESEA-Rice10: high-resolution annual paddy rice maps for Northeast and Southeast Asia from 2017 to 2019

Jichong Han et al.

Correspondence to: Zhao Zhang (sunny_zhang@bnu.edu.cn)

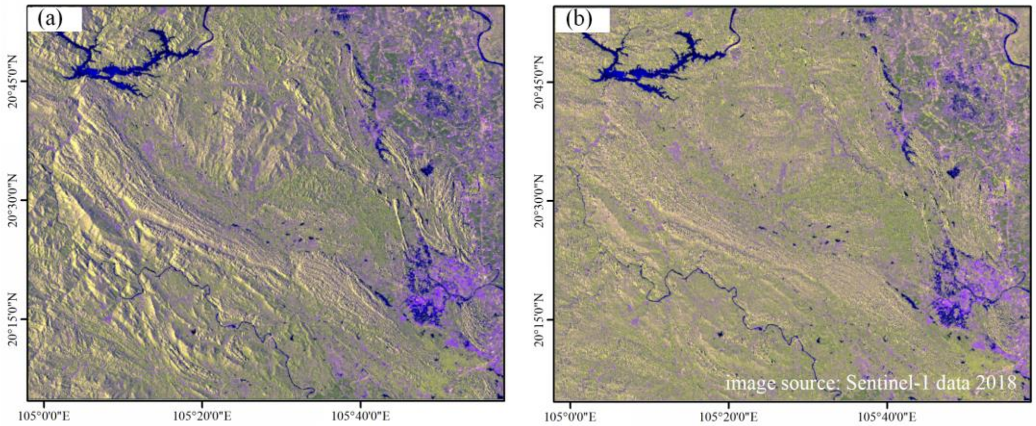

Figure S1. Sentinel-1 RGB color composite over the typical area in Vietnam in 2018 before correction (a) and after correction (b) with a physical volume model. (R/G/B: VV, VH, and VV/VH).

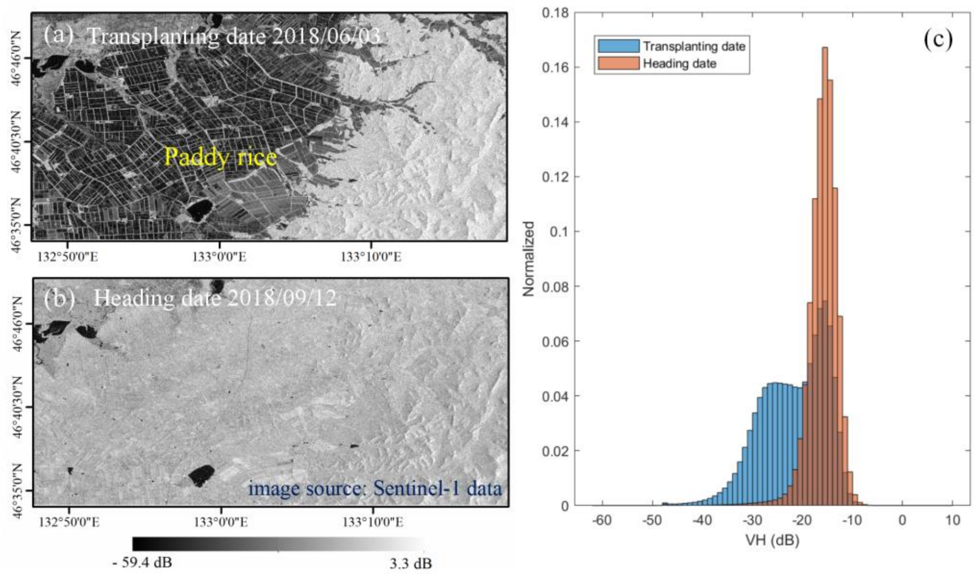

Figure S2. VH polarization backscatter images on the paddy rice transplanting date (a) and heading date (b), and normalized histogram of the images (c).

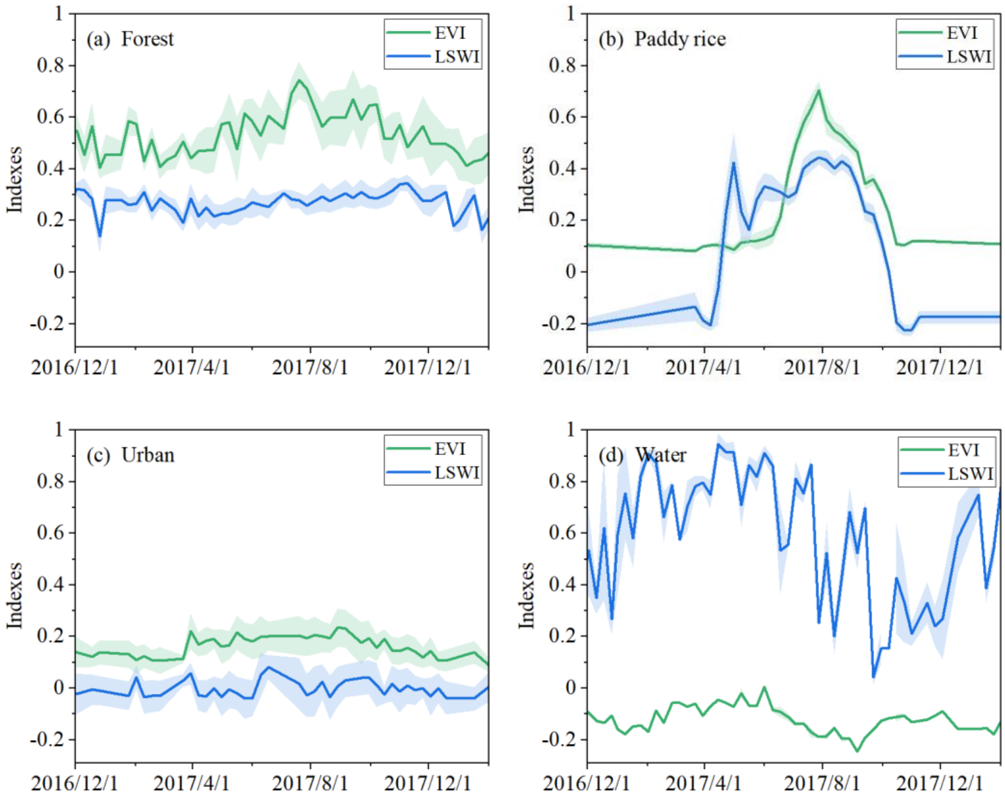

Figure S3. The seasonal dynamics of EVI and LSWI for different land cover types from random sample blocks. The profile was generated from the following random points: forest (20.232934°N, 103.552905°E), paddy rice (47.665726°N, 133.018530°E), urban (21.003088°N, 105.827390°E), water (12.974382°N, 103.940706°E). The light-shaded areas indicate the standard deviation.

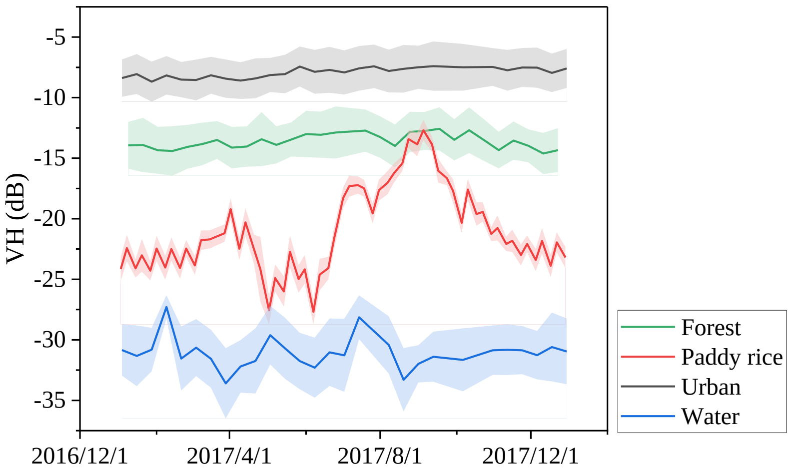

Figure S4. The seasonal dynamics of VH backscatter coefficients for different land cover types from random sample blocks with 100m radius. The profile was generated from the following random points: forest (20.232934°N, 103.552905°E), paddy rice (47.665726°N, 133.018530°E), urban (21.003088°N, 105.827390°E), water (12.974382°N, 103.940706°E). The light-shaded areas indicate the standard deviation.

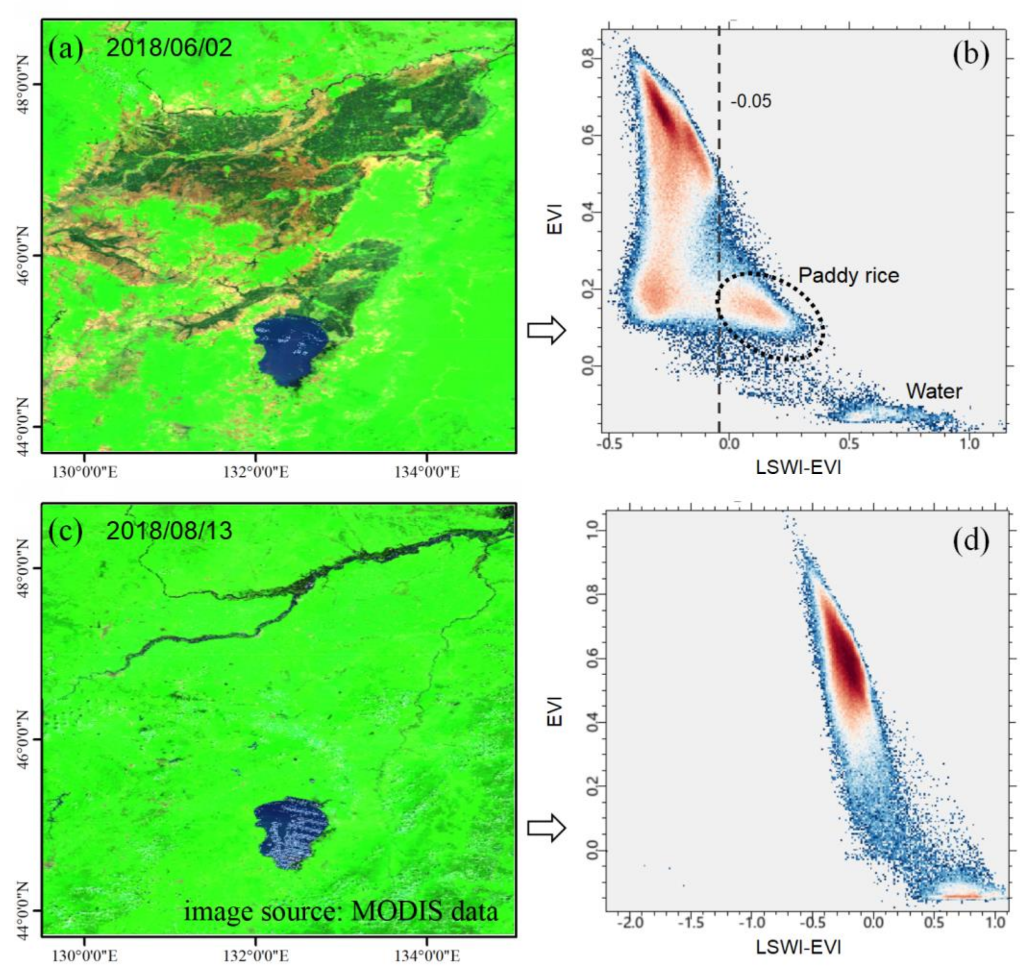

Figure S5. Spatial-temporal dynamics of flooded (a, b) and open canopy (c, d) for rice paddy fields in Northeast China. (a, c) Composite MODIS images displayed with SWIR2 band, NIR band, and blue band (R/G/B=band7/band2/band1). (b, d) the corresponding 2-D scatter plots of vegetation indices (EVI and LSWI) and the difference between them from the MODIS data. The color density represents the number of pixels.

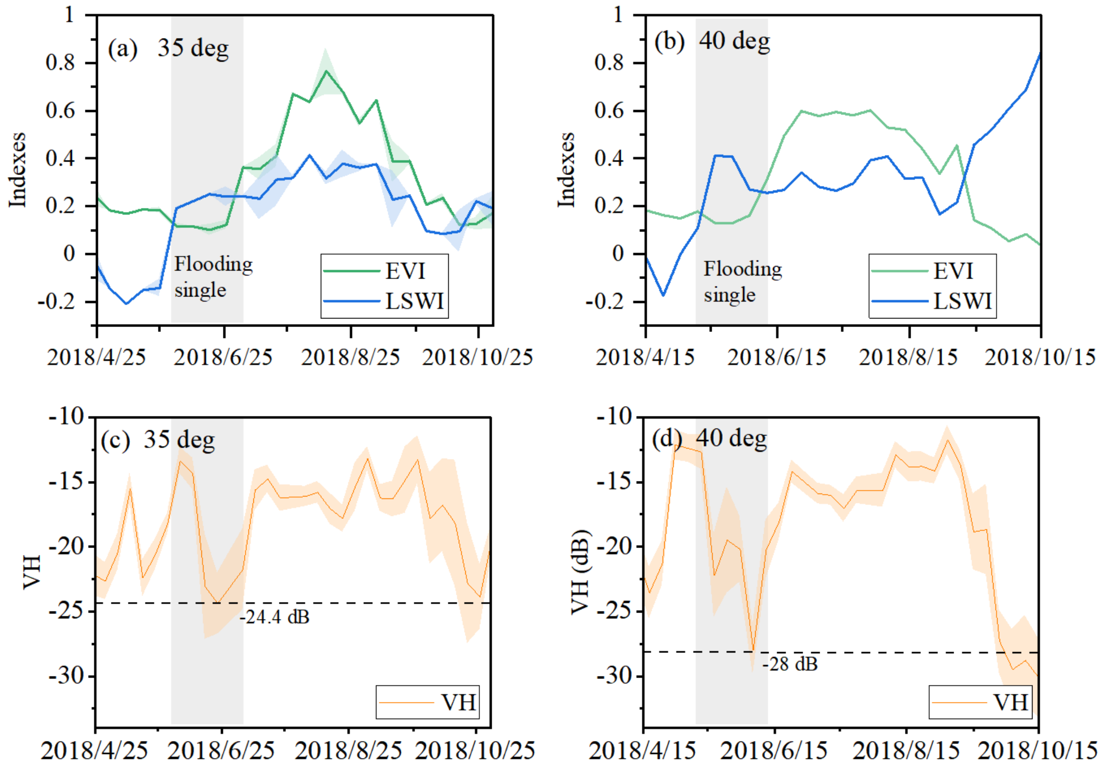

Figure S6. The seasonal dynamics of vegetation indices (EVI and LSWI) and backscattering coefficient (VH) of paddy rice at different incidence angles for Sentinel-1. (a, c) 35 deg. (b, d) 40 deg. The light-shaded areas indicate the standard deviation.

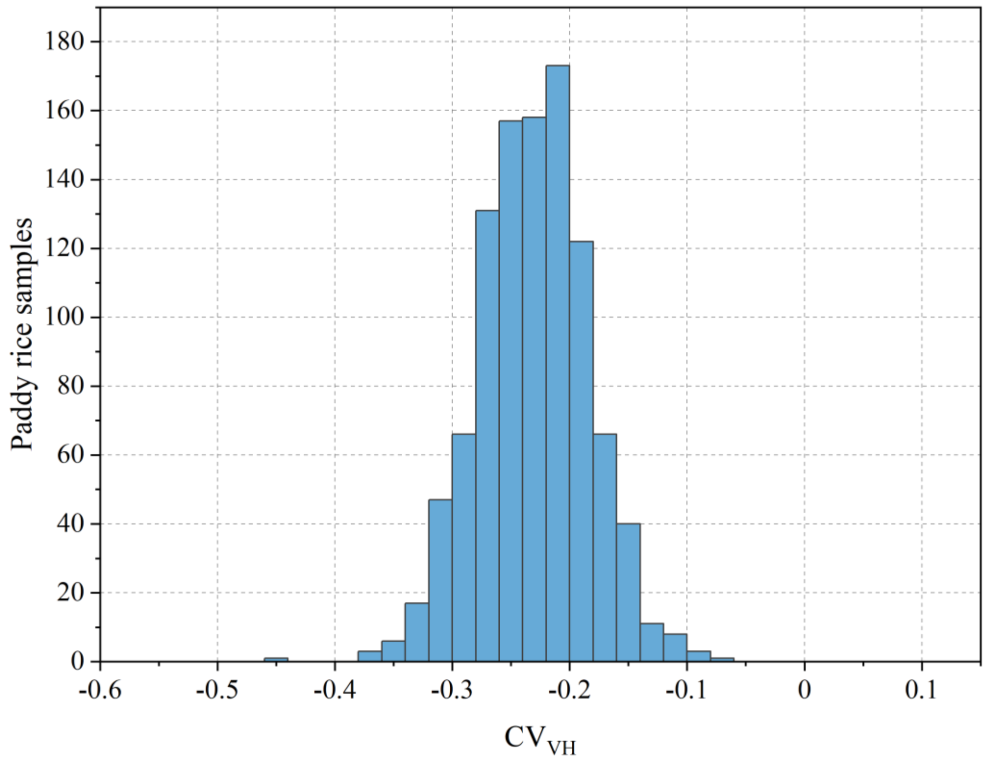

Figure S7. The histogram of the coefficient of variation of the time-series of VH (CV_{VH}) during the paddy rice growth period is based on sample rapeseed parcels in the study area.

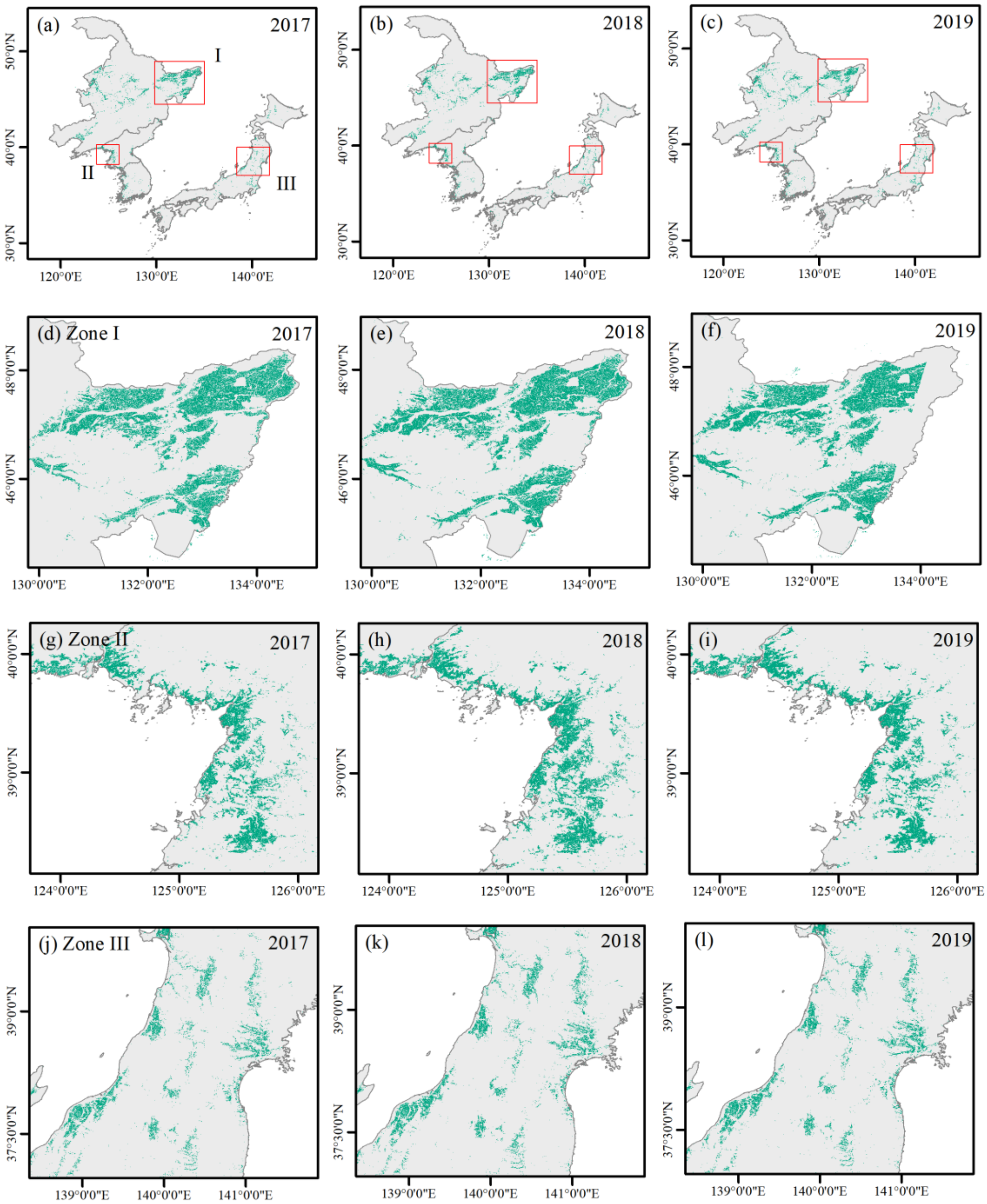

Figure S8. Spatial distribution of annual paddy rice fields with 10m resolution in Northeast Asia during 2017 - 2019 derived by our improved method (a-c). (d-l): the zoomed-in maps displaying detailed information in local zones. Find the example data for (d-l) here (https://doi.org/10.17632/cnc3tkbwcm.1 , example05-13).

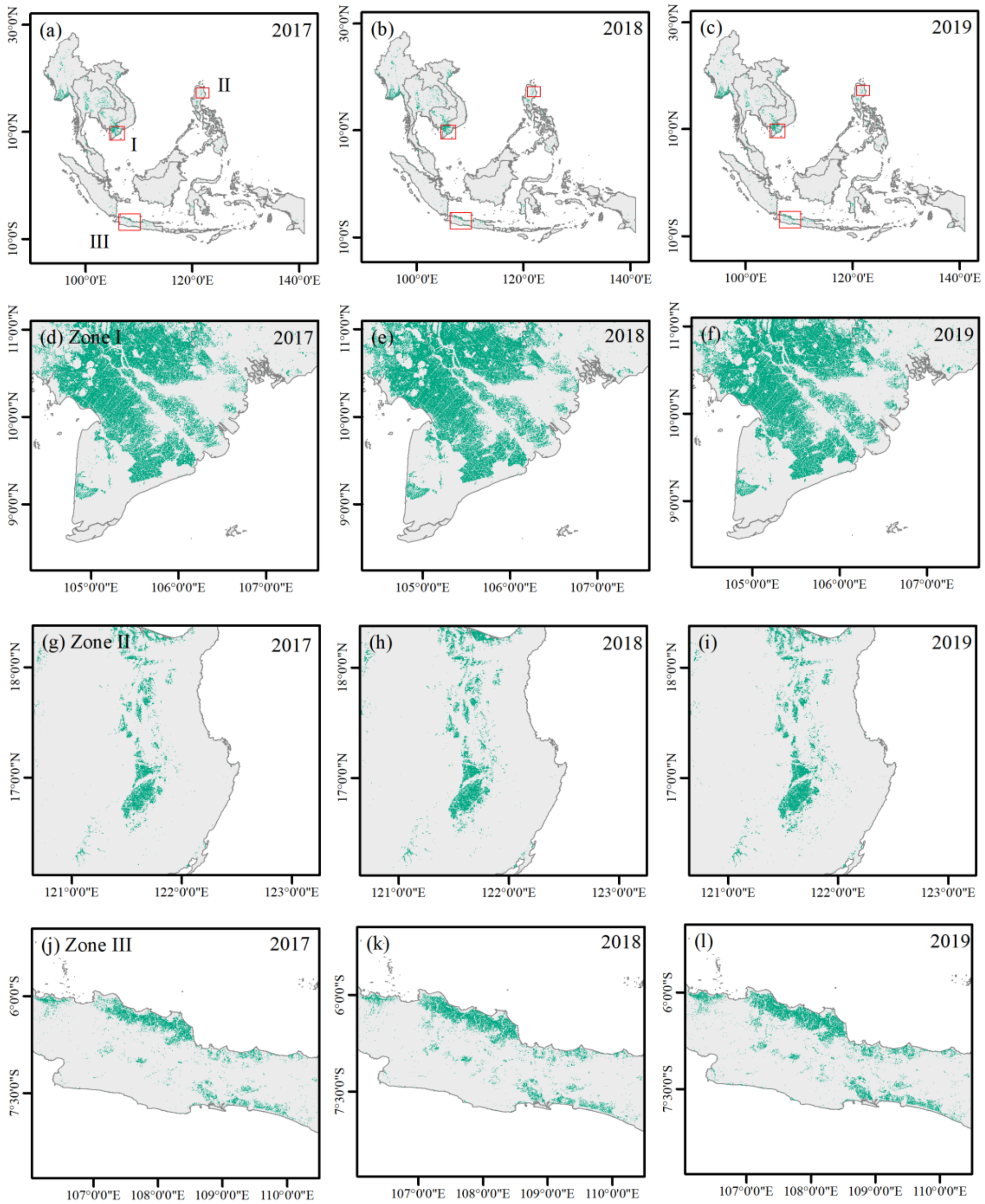

Figure S9. Spatial distribution of annual paddy rice fields with 10m resolution in Southeast Asia in 2017 - 2019 derived by our improved method (a-c). (d-l): the zoomed-in maps displaying detailed information in local zones. Find the example data for (d-l) here (https://doi.org/10.17632/cnc3tkbwcm.1 , example14-22).

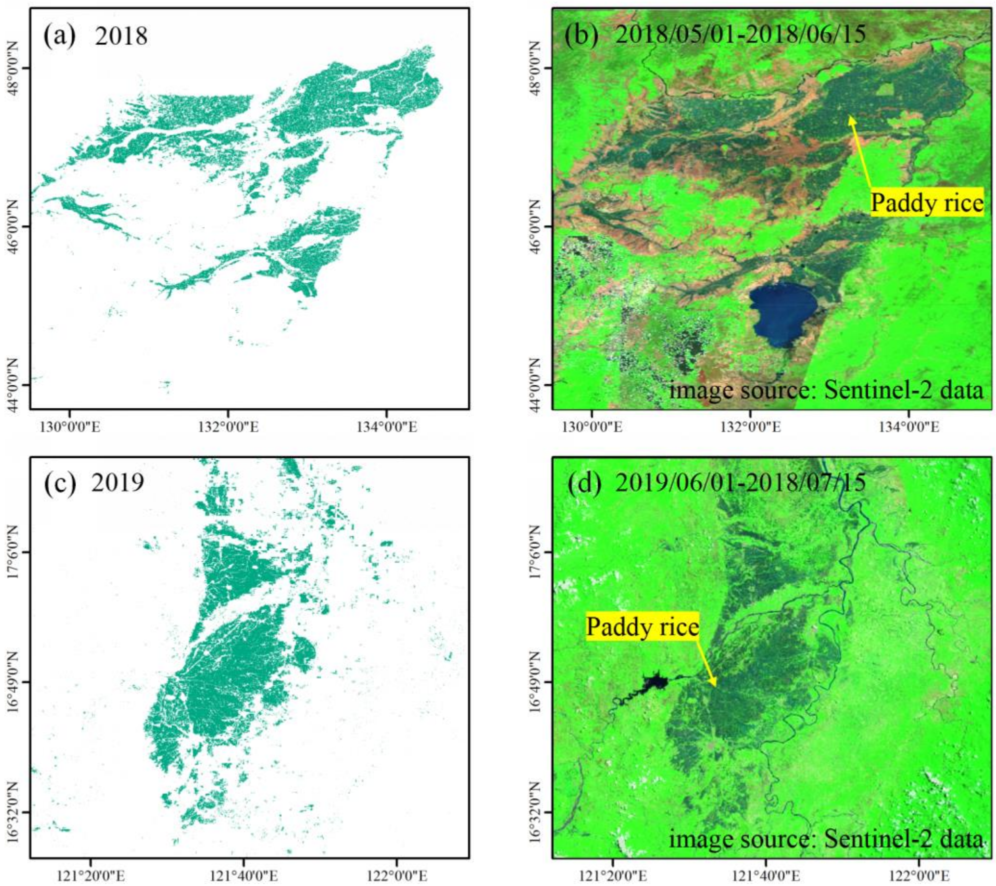

Figure S10. Comparison of classification results (a, c) with high-resolution optical images (b, d) from paddy rice transplanting period in typical areas. Sentinel-2 median images are composite displayed with SWIR2 band, NIR band, and blue band (R/G/B = band12/band8/band4).

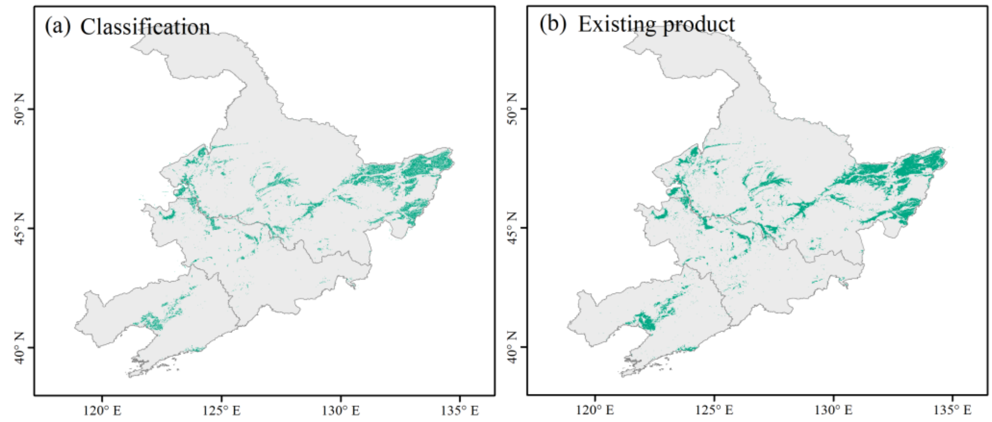

Figure S11. Comparison of our paddy rice map (a) with the existing MODIS-based map (b) in Northeast China in 2017.

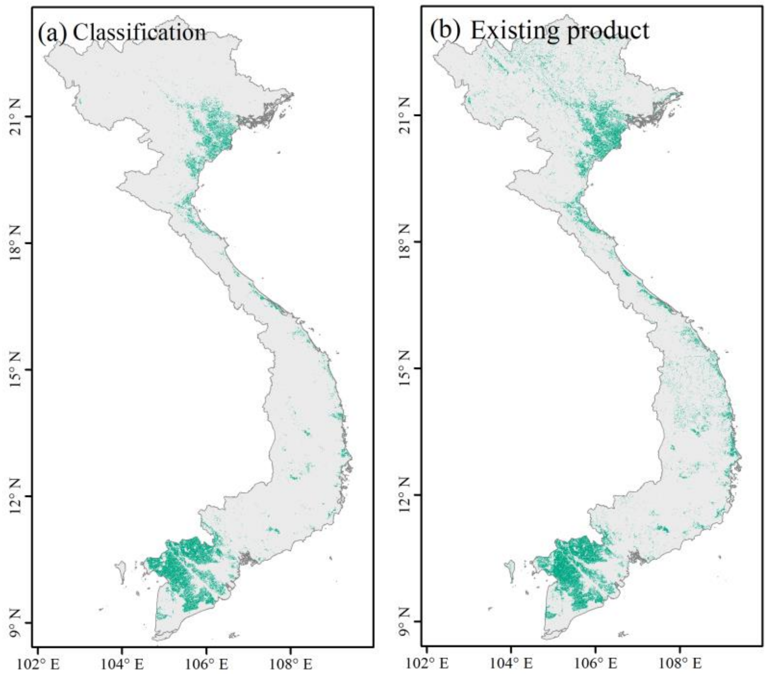

Figure S12. Comparison of our paddy rice map (a) with the existing map (b) (Paddy fields on the JAXA map) in Vietnam in 2017.

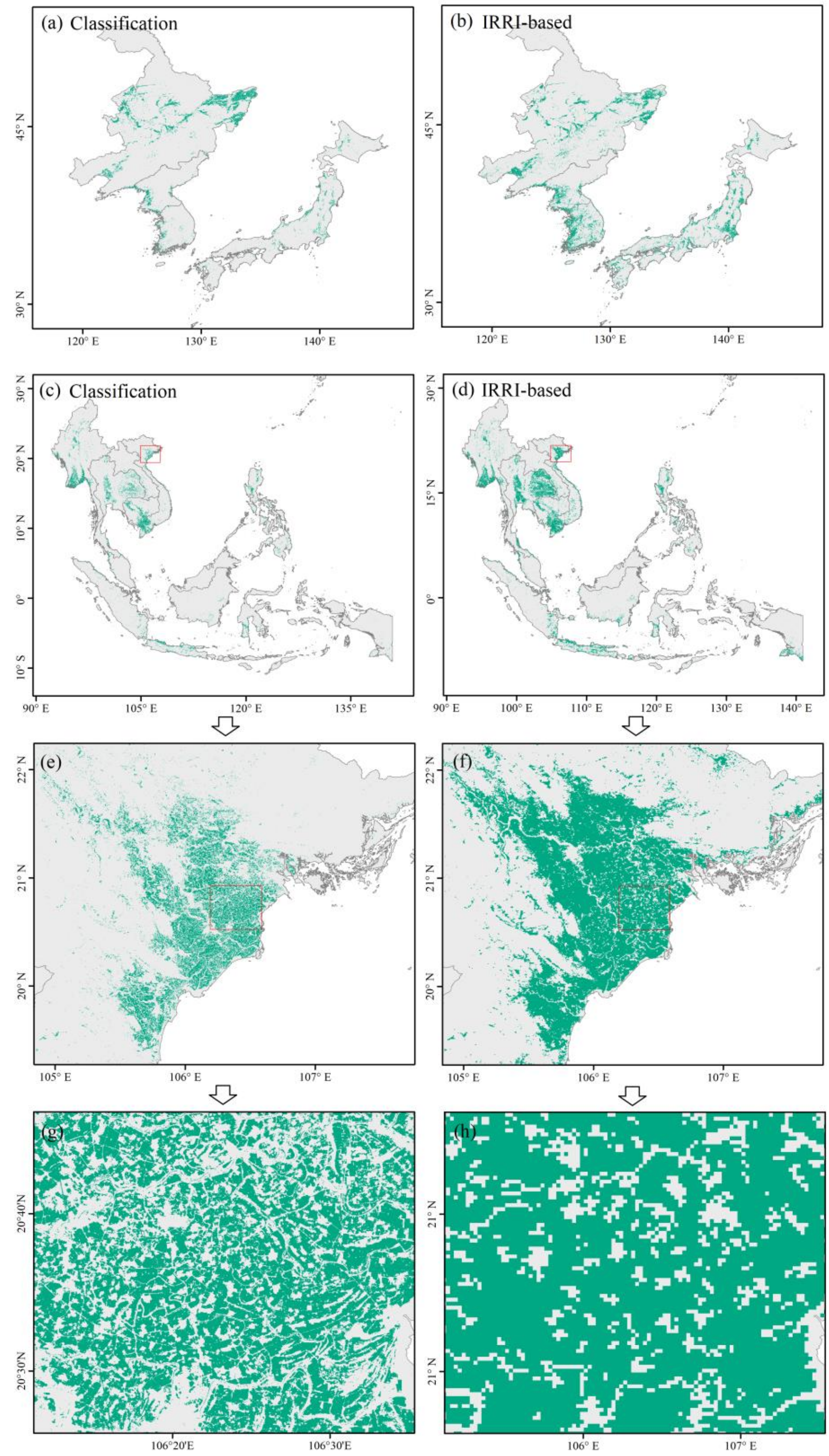

Figure S13. Paddy rice maps of Northeast and Southeast Asia. (a, c, e, and g) were derived by our method. (b, d, f, and h) are the International Rice Research Institute (IRRI)-based rice map. Note that the periods between our paddy rice maps (2017-2019) and the IRRI-based data products (2000-2012) are different. The purpose of the comparison is for a general verification of the paddy rice distribution.